Electrical Resistivity Behavior and VRH Transport Mechanism in Semiconducting La0.6Sr0.4Mn1–2x Fe x Cr x O3 (0.10≤x≤0.25) Manganites

Sonia Ben Abdelkhalek, Nabil Kallel, Sami Kallel, Thierry Guizouarn, Octavio Peña, Mohamed Oumezzine

Electrical resistivity behavior and VRH transport mechanism in semiconducting $La_{0.6}Sr_{0.4}Mn_{1-2x}Fe_xCr_xO_3$ ($0.10 \leq x \leq 0.25$) manganites

Sonia Ben Abdelkhalek[a], Nabil Kallel[a], Sami Kallel[a], Thierry Guizouarn[b], Octavio Peña[b], Mohamed Oumezzine[a]

[a] *Laboratoire de Physico-chimie des Matériaux, Département de Physique, Faculté des Sciences de Monastir, BP 22, 5019 Monastir, Tunisia*

[b] *Institut des Sciences Chimiques de Rennes, UMR 6226-CNRS, Université de Rennes 1, 35042 Rennes Cedex, France*

Abstract

The transport properties and conduction mechanism in $La_{0.6}Sr_{0.4}Mn_{1-2x}Fe_xCr_xO_3$ ($0 \leq x \leq 0.3$) have been investigated. The undoped samples show metal– semiconductor transition with a peak of resistivity at a temperature T_P, whereas for all doped compounds, the semiconducting behavior persists in the whole temperature range. The insertion of Cr^{3+} and Fe^{3+} ions leads to the increase of resistivity because the simultaneous substitution of Fe^{3+} and $Cr^{3+}$for Mn^{3+} reduces the number of available hopping sites for the Mn $e_{g\uparrow}$ electron and suppresses the double-exchange mechanism. It was found that the transport mechanism for substituted samples is dominated by the variable range hopping of small polarons between localized states model where the various parameters estimated from Mott's relation obey the variable range hopping (VRH) mechanism.

Keywords: Manganites, Electrical properties, conduction mechanism, VRH mechanism

***** Corresponding author: e-mail: abdk_sonia@yahoo.fr

Phone: +216 21093737, Fax: +216 73 500 278

1. Introduction

Since the discovery of many interesting phenomena in perovskite manganites such as colossal magnetoresistance (CMR), charge ordering, and orbital ordering, a great amount of effort has been devoted to understanding the unusual electronic and magnetic properties of these materials **[1–5]**. The Mn ions in mixed valence manganites $R_{1-x}A_xMnO_3$ (R-Rare earth elements, A-alkali or alkaline elements) play a crucial role in shaping the magnetic properties. The effect of Mn site doping by other transition elements (T = Ti, Cr, Fe, Co, Ni, Cu, Ru, etc.) or non-magnetic impurities like Al, Ga, i.e. $(La_{1-x}A_x)Mn_{1-y}T_yO_3$, has been studied by several groups of authors to understand the nature of magnetic interaction **[6–16]**. The doping at Mn site by other transition elements gives rise to changes in Mn^{3+}/Mn^{4+} ratio, which leads to complicated and interesting magnetic and electrical transport behavior and offer an unusual research opportunity for condensed matter physics. Such doping shows the following three effects: first, the doping ions reduce the number of hopping sites, and create cuts in the conduction path; second, the doping ions (or the doping ion and Mn ion) couple by superexchange, antiferromagnetically to the ferromagnetic Mn host lattice; and third, when the Mn sublattice is destabilized by substituting Mn by the other elements, the compounds result in inhomogeneous magnetic systems.

In this work, the choice of Cr^{3+} is based on the fact that its electronic structure is the same as that of Mn^{4+} ([Ar]$3d^3$). Its ionic radius (0.62 Å) is smaller than the one of Mn^{3+} (0.65 Å). For the Fe^{3+} ion, its ionic radius is close to the Mn^{3+} ionic radius **[17]**. Fe and Cr are the nearest neighbors of Mn in the Periodic Table and they are non-Jahn–Teller ions. Xiao et al. **[18]** suggest that there exists a poor DE interaction between Mn^{3+} and Cr^{3+} at high temperature so that Cr^{3+} cannot play the role of Mn^{4+} in the Mn^{3+}–O–Cr^{3+} interaction. Correspondingly, Cr^{3+} partially plays the role of Mn^{4+} in the low temperature range. However, other authors argued that Mn^{3+}–O–Cr^{3+} exchange interaction is super- exchange rather than DE **[19, 20]**. Regarding the identical ionic radii of Fe^{3+} and Mn^{3+}, Fe doping on the Mn-site can be selected in order to avoid lattice distortion. Thus the number of Mn^{3+}/Mn^{4+} is reduced, which hampers the DE mechanism forcing the change in electrical properties and influencing the polaronic transport. The electrical transports $\rho(T)$, have been studied extensively for the manganites **[21–25]**. The conduction mechanism in these materials is a matter of controversy as different schools of thought propose different conduction models. For example, in the semiconducting region, data on certain compounds were fitted with purely activated law **[26- 28]**. While some authors proposed small polaron hopping conduction mechanism (SPH) over extended temperature

ranges **[29-33]**, at the same time, Mott and Davies **[34, 35]** used the variable range hopping mechanism (VRH) for the whole temperature range.

Recently, we studied the structural and magnetic properties of $La_{0.6}Sr_{0.4}Mn_{1-2x}Fe_xCr_xO_3$ samples and the transport mechanisms were poorly studied **[36]**. In this paper we present the studies of electrical properties in these samples and we examine every transport model with more explication and details.

2- Experimental details

Powder samples of $La_{0.6}Sr_{0.4}Mn_{1-2x}Fe_xCr_xO_3$ were prepared using the solid-solid state reaction by mixing La_2O_3, Mn_2O_3, Fe_2O_3 and Cr_2O_3. The starting materials were intimately mixed in agate mortar for 1 h, and then heated in air at 1100 °C for 30 h. The powders were reground, pressed into pellets (of about 2 mm thickness and 6 mm diameters) and fired at 1200 °C for 30 h. This process was repeated at the same conditions to ensure a complete reaction. Finally, the powders are reground and sintered at 1280 °C in air for 96 h with intermediate grinding. The X-ray powder diffraction (XRD) patterns were recorded with a ‘‘PANalytical X’ert Pro’’ diffractometer with filtered (Ni filter) Cu radiation and $20° \leq \theta \leq 120°$. The magnetization was measured under a magnetic field of 0.01T using as upper conducting quantum interference device (SQUID) MPMS-XL5 ($2 \leq T \leq 400$ K). The temperature dependence of electrical resistivity ρ was measured by a conventional four-probe method in the temperature range 78–350 K with a typical sample size of 5 mm × 5 mm × 2 mm.

3. Results and discussion

3.1. General

X-ray diffraction data confirm all the samples as single phase materials without detectable secondary phases or impurity phases. The XRD data are successfully indexed with a rhomboheral ($R\bar{3}c$) structure. Fig. 1 shows an ordinary (observed) XRD pattern of x = 0.10 and x = 0.15 samples along with its Rietveld refined one and a curve showing the difference between both the patterns. As shown in Fig. 2, the magnetizations of samples with x = 0, 0.10, 0.15, 0.20 and 0.25 measured under an applied field of 0.01T exhibit a ferromagnetic to paramagnetic transition at T_C temperatures of 352, 215, 165, 125 and 100 K, respectively. We note that the Curie temperatures T_C have been determined from the intersection of the tangent to the inflection point of the M–T curve with its horizontal asymptote. As the Fe and Cr concentrations increase, the Curie temperature T_C decreases. This remarkable decrease of the Curie temperature T_C from 352 to 100 K in the presence of 25 % of Fe and 25 % of Cr is related to the decrease of rate of Mn^{3+} ions and the increase of concentration of Fe^{3+} and Cr^{3+}

ions. The partial substitution of Mn^{3+}, simultaneously replaced by Cr^{3+} and Fe^{3+}, causes a decrease of the $Mn^{3+/}Mn^{4+}$ ratio and decreases the number of hopping electrons and the available hopping sites between Mn^{3+} and Mn^{4+}, thus greatly weakening the double-exchange interaction of Mn^{3+}–O– Mn^{3+}. In the case of the partial replacement of Mn^{3+} by Cr^{3+}, the Mn^{3+}–O–Cr^{3+} super-exchange ferromagnetic interaction is weaker than the double-exchange interaction of Mn^{3+}–O–Mn^{4+}. In addition, there exists an anti-ferromagnetic Cr^{3+}–O–Cr^{3+} interaction **[37]**. On the other hand, when Mn^{3+} is partially substituted by Fe^{3+}, Mn ions can couple with neighboring Mn and Fe ions simultaneously, due to the strong antiferromagnetic Mn–Fe interaction. So the partial replacement of Mn^{3+} by Fe^{3+} can greatly weaken the double-exchange interaction of Mn^{3+}–O–Mn^{4+} and, therefore, the magnetic transition temperature T_C decreases.

Fig. 3 presents the temperature dependence of zero-field resistivity ρ for all the samples from 78 to 350 K. The undoped sample exhibits a ferromagnetic-metallic to paramagnetic–semiconductor transition at T_P = 315 K. For all the doped samples, the resistivity increases exponentially with decreasing temperature and shows a semiconducting behavior in the whole temperature range.

It can also be noticed from Fig. 3 that the resistivity increases with the coupled substitution of Mn^{3+} for Cr^{3+} and Fe^{3+}. This decrease in conductivity with Fe and Cr doping is considered to be associated with the decrease of the ratio Mn^{3+}/Mn^{4+}, which greatly weakens the influence of Mn^{3+}–O–Mn^{4+} double exchange (DE) interactions **[38, 39]**. The behavior of the samples can be explained by considering the electronic band structure of the material. The configuration of d electrons in transition metal oxides is determined by the internal crystal fields. In an octahedral field, the d levels split in to $t_{2g}\uparrow$, $e_g\uparrow$, $t_{2g}\downarrow$ and $e_g\downarrow$. The electronic configuration for Mn^{3+} is $t_{2g}^3 \uparrow e_g^1 \uparrow$ and for Mn^{4+} is $t_{2g}^3 \uparrow$, and electronic configuration for Fe^{3+} is $t_{2g}^3 \uparrow$ and $e_g^2 \uparrow$. Thus, the $e_g\uparrow$ band of Mn is electronically active, where electron hopping occurs between Mn^{3+} and Mn^{4+}. Simultaneous existence of Fe^{3+}, Mn^{3+} and Mn^{4+} indicates that the Fe $e_g\uparrow$ band is full and the Mn $e_g\uparrow$ band is half filled. The Fe $e_g\uparrow$ band remains fully filled only if the Mn $e_g\uparrow$ band has charge carriers. This implies that the bottom of the Mn $e_g\uparrow$ band should be at the same level as, or higher than, the top of the Fe $e_g\uparrow$ band. Consequently, the Fe $^{3+}$ cannot participate in electron hopping from Mn. The doping of Fe results in depletion in the number of hopping electrons and available hopping sites. Ahn et al. **[40]** and Jin et al. **[41]** suggested that Fe ions act as trapping centers for the e_g electrons and block the percolative hopping of the e_g electrons between the Mn^{3+} and Mn^{4+} ions. The

trapping centers perturb the double exchange mechanism. In addition, the presence of Fe^{3+} encourages the super-exchange interaction (Fe^{3+}–O–Mn^{4+}, Fe^{3+}–O–Mn^{3+} and Fe^{3+}–O–Fe^{3+}) against the double-exchange interaction (Mn^{3+}–O–Mn^{4+}), hence weakens the DE interaction, suppressing the metallic conduction and enhancing the semiconductor behavior. On the other hand, when the rate of substituted Cr^{3+} ions increases, the antiferromagnetic coupling between Cr^{3+}–Cr^{3+}, Cr^{3+}–Mn^{4+} and Mn^{4+}–Mn^{4+} should be taken into consideration. According to the work of Goodenough et al. **[42]**, we expect a weak antiferromagnetic superexchange interaction between two ions having an empty orbital e_g. With the increase of Cr^{3+} ions, the number of Mn^{3+} is reduced appreciably and the ferromagnetic double exchange interactions between Mn^{4+} and Mn^{3+} ions are weakened, while the antiferromagnetic interactions between Mn^{4+} and Cr^{3+} are reinforced. In addition to these antiferromagnetic interactions, there is a canting of the magnetic moments of the Fe and Cr ions, as observed in $La_{1-x}Nd_xFe_{0.5}Cr_{0.5}O3$ **[43]**.

Concerning the present work, the effect of Fe and Cr doping is the direct and simultaneous replacement of Mn^{3+} ions by Fe^{3+} and Cr^{3+} with a same content x. The increasing importance of the antiferromagnetic interactions Mn^{3+}–O–Fe^{3+}, Mn^{4+}–O–Fe^{3+}, Fe^{3+}–O–Fe^{3+}, Cr^{3+}–O–Mn^{4+} and Cr^{3+}–O–Cr^{3+}, Fe^{3+}–O–Cr^{3+} and the disorder introduced by the charge transfer weakens the double exchange interaction, enhancing the semiconducting behavior, which leads to the increase of resistivity.

3.2. Conduction mechanism

3.2.1. Metallic behavior for x = 0

In the metallic region ($T < T_P$) the following equations are generally used to fit the electrical resistivity data in case of the manganites,

$$\rho = \rho_0 + \rho_2 T^2 \quad (1)$$

$$\rho = \rho_0 + \rho_{2.5} T^{2.5} \quad (2)$$

$$\rho = \rho_0 + \rho_2 T^2 + \rho_{4.5} T^{4.5} \quad (3)$$

where ρ_0 is the resistivity due to grain/domain boundary and point defects scattering **[44,45]**, $\rho_2 T^2$ in Eqs.(1) and (3) represents the electrical resistivity due to the electron–electron scattering **[46]**. On the other hand $\rho_{2.5} T^{2.5}$ is the electrical resistivity due to electron–magnon scattering process in the ferromagnetic phase **[47]**. The term $\rho_{4.5} T^{4.5}$ is a combination of electron–electron, electron–magnon and electron–phonon scattering processes **[48, 49]**. The $T < T_P$ experimental data for x = 0 sample was fitted to the above three equations and the quality of these fittings, in general, is evaluated by comparing the square of correlation coefficient (R^2) obtained for each equation. The fit values (square of the correlation

coefficient, R^2) for equations (1)-(3) are given in Table1. Best results are obtained using Eq. (3). The data and their corresponding fit based on equation (3) are shown in Fig. 4. The fit parameters obtained from Eq.(3), ρ_0, ρ_2 and $\rho_{4.5}$, have values of 0.0015 Ω cm, 3.117×10^{-8} Ω cm K^{-2}, -8.4094×10^{-15} Ω cm $K^{-4.5}$, respectively.

3.2.2. Semiconducting behavior for all doped samples

Many attempts were made to explain the variation of the electrical resistivity with temperature in the case of manganites. In the semi-conductor region, thermal activation **[26]** process, hopping motion of small polarons **[29]** and variable range hopping mechanism **[50]** etc., can fit the resistivity.

3.2.2.1. Thermal activation model (TA)

For crystalline semiconductors with a well-defined energy gap, the activated character may be determined by the thermal activation of electrons from the valence band to the conduction band (intrinsic conductivity) or from the impurity levels (impurity conduction). Thermally activated hopping transport may also occur when the carriers are lattice vibrations or magnetic polarons **[51]**. If the thermal energy is sufficient to overcome the bandgap the electron becomes free to conduct. The expression for resistivity can be written in the following form:

$$\rho = \rho_0 \exp (E_A/k_B T) , \qquad (4)$$

where T is the absolute temperature, ρ_0 the value of resistivity at infinite temperature, E_A the activation energy and k_B the Boltzmann's constant, i.e., for the bandgap model the graph must exhibit Arrhenius temperature dependence (straight line behavior between log ρ and 1/T). Our experimental data for all doped samples (x = 0.10, 0.15, 0.20 and 0.25) were fitted using eq. 4 (Fig. 5). The R correlation factor and the activation energy E_a for the TA model are given in Table 2. The thermal activation model poorly describes our results in the semi-conducting region for all samples and hence we conclude that the thermal activation model is insufficient to explain the conduction process of this material.

3.2.2.2. Small polaron hopping model

Our experimental data were also fitted using adiabatic nearest-neighbor hopping of small-polarons (Holstein polaron) model (ANHSP), which leads to a mobility of a thermally activated form. In the adiabatic regime the charge-carrier motion is faster than the lattice vibrations, and the drift mobility is given by $\mu = (\frac{3ea^2}{2})(\frac{\upsilon_0}{2\pi k_B T})\exp(\frac{-W_p}{k_B T})$ where $W_p = \frac{E_p}{2-t}$.

E_p denotes the polaron formation energy, (t) the electronic transfer integral, (υ_0) the

longitudinal optical-phonon frequency, (*a*) the hopping distance, and (*e*) the electronic charge. Adiabatic nearest-neighbor hopping of small-polarons model **[52]** is given by:

$\rho = \rho_0 T \exp(E_{hop}/k_B T)$ (5)

where E_{hop} is the hopping energy, k_B the Boltzmann constant and ρ_0 the resistivity coefficient and is given by:

$\rho_0 = 2k_B/3ne^2a^2v$ (6)

here *e* is electronic charge, *n* is number of density of charge carriers, *a* is site-to-site hopping distance, and *v* is longitudinal optical phonon frequency.

Further, in order to check whether the conduction process obeys ANSPH, a graph is plotted with log (ρ/T) on the *Y* – axis and 1/*T* on the X – axis (figure 6). We should notice that there is an apparent change in the slope of the resistivity near the magnetic ordering temperature T_C (T_C = 215, 165, 125 and 100 K for x = 0.10, 0.15, 0.20 and 0.25 respectively) (Fig. 6), which indicates a close correlation between the magnetic state and the transport behavior and justifies that the onset of the ferromagnetic exchange interaction promotes the transfer of charge carriers. A change in the slope was also observed in $LaMn_{1-x}Cr_xO_3$ **[53]** and $La_{1-x}Nd_xMn_{0.8}Cr_{0.2}O_3$ **[54]**. From such fits we obtain the hopping energy E_{hop}, the resistivity coefficient ρ_0 and the correlation factor R (see Table 2 for the ANHSP model). Fig. 6 shows the results for this model, in which the straight lines are fits to the adiabatic small polaron hopping model. From Table 2, we find that the E_{hop} increases with increasing *x*, while the resistivity coefficient ρ_0 shows a complex correlation as a function of *x*, first decreasing from $0.555\ 10^{-4}$ to $0.453\ 10^{-4}$ Ωcm/K (from x = 0.10 to x = 0.15) and then increasing up to $9.02\ 10^{-4}$ Ωcm/K for x = 0.25. It is possible that ρ_0 varies with Fe and Cr doping due to the variation in either *n* (the polaron concentration) or *a* (the hopping distance). In fact, replacing Jahn–Teller Mn^{3+} ions by non-Jahn–Teller Fe^{3+} and Cr^{3+} ions will lead to a decrease in the polaron concentration *n* **[55, 56]**. As the e_g shell of Fe^{3+} is completely filled, the charge carriers cannot pass through the Fe^{3+} sites due to the strong Coulomb repulsion. Hence, Fe ions act as trapping centers for the e_g electrons and block the percolative hopping of the e_g electrons between the Mn^{3+} and Mn^{4+} ions. In addition, the presence of Cr^{3+} generates antiferromagnetic interactions through Cr^{3+}-O-Cr^{3+} and Cr^{3+}-O-Mn^{4+} which cannot participate in double exchange mechanism. In this case, the carriers must detour or hop over these enhanced barriers due to Fe and Cr doping, so the average hopping distance (*a*) increases with *x*. For *x* = 0.10–0.15, the change of polaron concentration *n* is relatively small, so the decrease of ρ_0 with *x* is due to the increase of the hopping distance (*a*). However, when the doping level is high enough (x = 0.20, 0.25), the change in the carrier concentration overcomes the

effect of the increasing hopping distance because (*a*) has an upper limit due to the finite activation energy of the polaron. As a consequence, na^2 drops down even if (*a*) grows, causing ρ_0 to increase. These results are similar to other electrical studies for substituted manganites in B site **[55, 57]**.

As we said above, the polaron would hop to sites further away than nearest neighbors if there are enough on-site barriers due to the Fe and Cr doping. Because of random distribution of polaron and disorder introduced by the presence of Cr and Fe ions, the dominating transport process in the $La_{0.6}Sr_{0.4}Mn_{1-2x}Fe_xCr_xO_3$ (x = 0.10, 0.15, 0.20, 0.25) samples could be a combination of polaron nearest-neighbor hopping and non-nearest-neighbor hopping **[55, 57]**. This means that the present adiabatic nearest-neighbor hopping model of small polarons (Holstein theory) is not satisfactory to explain the electrical behavior of our doped samples. Indeed, the Holstein theory of small polaron based on the molecular-crystal model was originally proposed for an ordered situation in which all the lattice sites were energetically equivalent, a situation which is not satisfied in $La_{0.6}Sr_{0.4}Mn_{1-2x}Fe_xCr_xO_3$ due to the strong electrical and magnetic disorder induced by Fe^{3+} and Cr^{3+} doping. In our case, the thermal energy is not large enough to allow electrons to hop to their nearest-neighbors and it becomes more favorable for the electrons to hop further to find a site with a smaller potential difference. Thus, this model, known as the variable range hopping model of small polarons (VRH) **[58]**, seems to apply better to our case, as we discuss below.

3.2.2.3. Variable range hopping

Assuming now that the electrical transport in the semiconducting phase proceeds via the Mott VRH variable range hopping mechanism: In the case of the disordered magnetic phase when the carriers are localized by random potential fluctuations, the temperature dependence of ρ in zero field is explained mainly by Mott's VRH expression **[50]**:

$$\rho \approx \rho_0 \exp\left(\frac{T_0}{T}\right)^{1/4} \qquad (7)$$

where, ρ_0 depends on the assumption made about the electron–phonon interaction and is considered as a constant in most of the cases although slightly affected by temperature, T_0 is the characteristic temperature of the compound, this parameter is proportional to the Mott localization energy and is expressed functionally as:

$$T_0 = \frac{\lambda \alpha^3}{k_B N(E_F)} \qquad (8)$$

where $\lambda(\cong 18)$ is a dimensionless constant, $N(E_F)$ is the density of states and α corresponds to the inverse of localization length (1/ζ). Figures 7 show the plots of Log $\rho \sim (1/T)^{1/4}$ revealing good concurrence with VRH model. As shown in Table 2, the VRH mechanism gives the best fit and the best correlation factor R among all models treated in this work. These results suggest that the dominant transport mechanism is a variable range hopping. Furthermore, the correlation factor R increase while increasing the Fe and Cr concentration and reaches 0.99995 for x = 0.25, this indicate that the replacement of Mn^{3+} sites by Fe and Cr ions promotes the VRH model in these samples.

The density of states at Fermi level $N(E_F)$ is calculated from the slope of Log(ρ) vs. $T^{-1/4}$ plot. While making these calculations, α value was taken as 2.22 nm^{-1} **[59-61]**. The estimated values of T_0 and $N(E_F)$ are given in Table 1. It can be seen from the table that the calculated values of $N(E_F)$ are found to be very close to the reported ones **[62]**. It is also clear from Table 2 and inset in figure 7 that the values of T_0 are found to increase. Obviously, when adding Fe and Cr, the e_g electrons of Mn^{3+} ions become localized, which increases the Mott localization energy as well as T_0. This is due to the decrease of Mn^{3+} ions and weakening of double exchange interactions as well as the magnetic disorder which becomes stronger by increasing the rates of Fe and Cr. The magnetic disorder introduced by the random distribution of Fe and Cr ions prevent the electrons transfer to their nearest-neighbors, which are on-site barriers due to the Fe and Cr doping, destroying the way of itinerant electron between Mn^{3+} and Mn^{4+}. In this disordered situation, the sites are not energetically equivalent and it becomes more favorable for the electrons to hop further this site barrier to find a site with a smaller potential difference. Hence, this mechanism is called variable range hopping (VRH).

We now consider two other parameters: the average hopping distance (a) and the average hopping energy (W), given by **[63]**:

$$a = \left[\frac{9}{8\pi \alpha k_B T N(E_F)} \right]^{1/4} \qquad (9)$$

$$W = \left[\frac{3}{4\pi a^3 N(E_F)} \right] \qquad (10)$$

This formula can be written also in a universal form $W = K_B T^{3/4} T_0^{1/4}$.

Using formula (10), the estimated values of W for x = 0.10, 0.15, 0.20 and 0.25 are shown in Fig. 8(a) as a function of temperature. The increase of T_0 and the decrease of $N(E_F)$ with the Fe concentration (Table 1) lead to the increase of the average hopping energy W. In fact, when adding Fe and Cr, the e_g electrons of Mn^{3+} ions become localized, since the Fe^{3+} ions

act as barriers to the charge carriers, thus increasing W. When the rate reaches 25 % Fe and 25 % Cr, the e_g electrons of the Mn^{3+} ions are more localized and the hopping energy becomes very large. In this case, it is energetically favorable for a localized carrier to hop to a site beyond the nearest-neighbor centers, which are on-site barriers due to the Fe and Cr doping. Then the average hopping length exceeds the average distance between the sites and consequently, the hopping distance (*a*) increases with increasing Fe and Cr doping, as shown in Fig. 8(b) when using formula (9). At room temperature, the average hopping distance (*a*) values are 1.46, 1.82, 2.55, 2.67 nm (figure 8(b)) respectively for x = 0.10, 0.15, 0.20, 0.25. Since, for variable range hopping model, the hopping distance must exceed Mn-Mn distance (In our case, Mn-Mn distance obtained by Rietveld analysis is 0.33 nm for undoped sample) and should be several times greater **[46]**, thus, these numbers of hopping distance are physically plausible and compatible with conventional variable-range hopping. Similar results are obtained by viret et al. **[46]** where the average hopping distance are 3–4 times the Mn-Mn separation. As shown in Figure 8(b), the hopping distance (a) decreases with increasing temperatures. On the other hand, the hopping energy *W* (figure 8(a)) increases with increasing temperature. This indicates that disorder plays a key role in the high temperature ($T > T_C$) conduction process, that is, the conduction mechanism in the semiconducting phase is dominated by the VRH mechanism **[64]**. Furthermore, When (αa) > 1 and $W >> k_BT$ the VRH is always to be expected **[65]**. Thus, all these results: increase in T_0 and decrease in the density of states at the Fermi level, increase in the average hopping energy *W* and of the hopping distance *a* when increasing the Fe content, show that the mechanism of conduction in these samples obeys to the variable range hopping (VRH) between localized states.

4. Conclusion

Single phases of $La_{0.6}Sr_{0.4}Mn_{1-2x}Fe_xCr_xO_3$ ($0 \leq x \leq 0.25$) have been prepared using a ceramic method. The low temperature resistivity measurements in the temperature regime were carried out. The undoped sample exhibits a ferromagnetic-metallic to paramagnetic– semiconductor transition. The resistivity shows semiconducting features for all doped compounds. The insertion of Cr^{3+} and Fe^{3+} ions in the parent compound $La_{0.6}Sr_{0.4}MnO_3$ leads to an increase of the resistivity. This may be due to the reduction of available hopping sites number for the Mn $e_{g\uparrow}$ electron and suppression of double-exchange mechanism. The data thus obtained for x = 0.10, 0.15, 0.20, 0.25 were fitted systematically to check the dominance of one particular mechanism over another viz. thermal activation (TA) model, adiabatic nearest-neighbor hopping of small-polarons (Holstein polaron) (ANHSP) model and the variable range hopping

(VRH). The fits show that the electronic transport in semiconducting $La_{0.6}Sr_{0.4}Mn_{1-2x}Fe_xCr_xO_3$ (x = 0.10, 0.15, 0.20, 0.25) is well described and dominated by the variable range hopping mechanism where the various parameters estimated from Mott's relation obey the VRH mechanism.

References

[1] S. Jin, T.H. Tifefel, M. McCormack, R.A. Fastnacht, R. Ramessh, L.H. Chen, Science 264 (1994) 413.

[2] A. Asamitsu, Y. Moritomo, Y. Tomioka, H. Kuwahara, Y. Tokura, Nature 373 (1995) 407.

[3] T.Y. Tyson, J. Mustre de Leon, S.D. Conradson, A.R. Bishop, J.J. Neumeier, H. Ro¨der, J. Zang, Phys. Rev. B 53 (1996) 13958.

[4] P. Schiffer, A.P. Ramirez, W. Bao, S.W. Cheong, Phys. Rev. Lett. 75 (1995) 3336.

[5] H.Y. Hwang, S.W. Cheong, P.G. Radaelli, M. Marezio, B. Batlogg, Phys. Rev. Lett. 75 (1995) 914.

[6] N. Kallel, S. Ben Abdelkhalek, S. Kallel, O. Pena, M. Oumezzine, J. Alloys Compd. 501 (2010) 30.

[7] Song, H., Kim, W., Kwon, S.-J., Kang, J.: J. Appl. Phys. **89**, 3398 (2001)

[8] Tai, M.F., Lee, F.Y., Shi, J.B.: J. Magn. Magn. Mater. **209**, 148 (2000)

[9] Troyanchuk, I.O., Lobanovsky, L.S., Khalyavin, D.D., Pastushonok, S.N., Szymczak, H.: J. Magn. Magn. Mater. 210, 63 (2000)

[10] Khalyavin, D.D., Pekala, M., Bychkov, G.L., Shiryaev, S.V., Barilo, S.N., Troyanchuk, I.O., Mucha, J., Misiorek, H., Szymczak, R., Baran, M., Szymczak, H.: J. Phys., Condens. Matter 15, 925 (2003)

[11] Shi, J.B., Fan, Y.Y., Tai, M.F., Chen, H.Z., Young, S.L.: J. Magn. Magn. Mater. 239, 8 (2002)

[12] Pollert, E., Hejtmanek, J., Jirak, Z., Knizek, K., Marysko, M., Doumerc, J.P., Grenier, J.C., Etourneau, J.: J. Solid State Chem. **177**, 4564 (2004)

[13] M.T. Tlili, M. Bejar, E. Dhahri, M. Sajieddine, M.A. Valente, E.K. Hlil, Materials Characterization, 62, 243 (2011)

[14] Srivastava, C.M., Banerjee, S., Gundu rao, T.K., Nigam, A.K., Bahadur, D.: J. Phys. Condens. Matter **15**, 2375 (2003)

[15] Wu, B.M., Li, B., Zhen, W.H., Ausloos, M., Du, Y.L., Fagnard, J.F., Vanderbemden, Ph.: J. Appl. Phys. **97**, 103908 (2005)

[16] Gao, H.P., Wu, B.M., Li, B.: Physica B **389**, 252 (2007)

[17] R.D. Shannon, Acta Crystallogr. Sect. A. 32 (1976) 75.

[18] X. Xiao, S.L. Yuan, Y.Q. Wang, G.M. Ren, J.H. Miao, G.Q. Yu, Z.M. Tian, L. Liu, L. Chen, S.Y. Yin, Solid State Commun. 141 (2007) 348.

[19] R. Gundakaram, Anthony Arulraj, P.V. Vanitha, C.N.R. Rao, N. Gayathri, A.K. Raychaudhuri, A.K. Cheetham, J. Solid State Chem. 127 (1996) 345.
[20] O. Cabeza, M. Long, C. Severace, M.A. Bari, C.M. Muirhead, M.G. Francesconi, C. Greaves, J. Phys.: Condens. Matter 11 (1999) 2569.
[21] K. Padmavathi, G. Venkataiah, P. Venugopal Reddy, J. Magn. Magn. Mater 309 (2007) 237.
[22] M.F. Mostafa, S.S. Ata-Allah, A.A.A. Youssef, H.S. Refai, J. Magn. Magn. Mater. 320 (2008) 344
[23] Xiaojuan Li, QiangWang, Physica B 404 (2009) 3703
[24] S.K. Srivastava · S. Ravi, J. Supercond. Nov. Magn 22 (2009) 651
[25] D. S. Rana, C. M. Thaker, K. R. Mavani, and D. G. Kuberkar, Darshan C. Kundaliya and S. K. Malik, J. Appl. Phys. 95 (2004) 4934
[26] Kusters R M, Singleton J, Keen D A, McGreevy R, Hayes W. Physica B 155 (1989) 362
[27] M. F. Hundley, M. Hawley, R. H. Heffner, Q. X. Jia, J. J. Neumeier, J. Tesmer, J. D. Thompson, and X. D. Wu, Appl. Phys. Lett 67 (1995) 860.
[28] G.C Xiong, S.M Bhagat, Q Li, M Domínguez, H.L Ju, R.L Greene, T Venkatesan, Jeff M Byers, Mark Rubinstein, Solid State Commun. 97 (1996) 599.
[29] Holstein T, Ann. Phys. 8 **(**1959) 325.
[30] Jakob G, Westerburg W, Martin F and Adrian H, Phys. Rev.B58 **(**1988) 14966.
[31] Snyder G J, Hiskes R, Dicarolis S, Beasley M R, Geballe T H, Phys. Rev B53 (1996) 14434.
[32] Yeh N C, Vasquez R, Beam D, Fu C C, Huynh H, Beach G, J. Phys.: Condens. Matter 9 (1996) 3713
[33] N.-C. Yeh, R. P. Vasquez, C.-C. Fu, J. Y. T. Wei, J Huynh, G. Beach, and D. A. Beam, J. Appl. Phys. 81, 5499 (1997).
[34] N. F. Mott, Metal–insulator transitions 1990 (London: Taylor and Francis)
[35] N. F. Mott and E. A. Davies, Electronic processes in noncrystalline materials 1971 (Oxford University Press)
[36] S. Ben Abdelkhalek, N. Kallel, S. Kallel, T. Guizouarn, O. Peña and M. Oumezzine, J. Magn. Magn. Mater, 322 (2010) 3416–3422
[37] R. Gundakaram, A. Arulraj, P.V. Vanitha, C.N.R. Rao, J. Solid State Chem. 120 (1995) 204.
[38] Z.M. Wanga, G. Ni, H. Sanga, Y.W. Dua, J. Magn. Magn. Mater. 234 (2001) 213.

[39] S. Bhattacharya, S. Pal, R.K. Mukherjee, B.K. Chaudhuri, S. Neeleshwar, Y.Y. Chen, S. Mollah, H.D. Yang, J. Magn. Magn. Mater. 269 (2004) 359.
[40] K.H. Ahn., X.W. Wu, K. Liu, C.L. Chien, Phy. Rev. B 54 (1996) 15299
[41] K.X. Jin, S.G. Zhao, J. Tang, C.L. Chen, J. Alloys Compd. 476 (2009) 765.
[42] J.B. Goodenough, A. Wold, R.J. Arnott, N. Menyuk, Phys. Rev. 124 (1961) 373.
[43] M. Tseggai, P. Nordblad, R. Tellgren, H. Rundlöf, A. K. Azad, S. G. Eriksson, J. Eriksen, J. Alloys Compd. 458 (2008) 372.
[44] A. Urushibara, Y. Moritomo, T. Arima, A. Asamitsu, G. Kido, Y. Tokura, Phys. Rev. B 51 (1995) 14103.
[45] D.C. Worledge, G.J. Snyder, M.R. Beasley, T.H. Geballe, J. Appl. Phys. 80 (1996) 5158.
[46] M. Viret, L. Ranno, J.M.D. Coey, Phys. Rev. B 55 (1997) 8067.
[47] V. Sen, N. Panwar, G.L. Bhalla, S.K. Agarwall, J. Phys. Chem. Solids 68 (2007) 1685.
[48] G.J. Snyder, R. Hiskers, S. DiCarolis, M.R. Beasley, T.H. Geballe, Phys. Rev. B 53 (1996) 14434.
[49] G. Venkataiah, P. Venugopal Reddy, Solid State Comm. 136 (2005) 114.
[50] N. Mott, in: Conduction in Non-Crystalline materials, Clarendon, Oxford, 1993, pp. 17–23.
[51] N.F. Mott, E.A. Davies, Electron Processes in Non-crystalline Materials, Clarendon, Oxford, 1979.
[52] D. Emin, et al., Ann. Phys. 53 (1969) 439.
[53] Y. Sun, W. Tong, X. Xu, Y. Zhang, Phys. Rev. B 63 (2001) 174438.
[54] Da-Qian Liao, Young Sun, Ren-Fu Yang, Zhao-Hua Cheng, Physica B 394 (2007) 104.
[55] Sun Y, Xu X J, Zheng L and Zhang Y H, Phys. Rev. B **60** (1999)12 317
[56] M.S. Sahasrabudhe, S.I. Patil, S.K. Date, K.P. Adhi, S.D. Kulkarni, P.A. Joy, R.N. Bathe, Solid state communications 137 (2006) 595
[57] Q. Huang, Z. W. Li, J. Li, and C. K.ong, J. Phys: Condens.Matter.13, 4033(2001)
[58] R. Laiho, K.G. Lisunov, E. Lahderanta, V.N. Stamov, V.S. Zakhvalinskii, J. Phys.: Condens. Matter 13 (2001) 1233.
[59] S. Pal, A. Banerjee, E. Rozenberg, B.K. Chaudhuri, J. Appl. Phys. 89 (2001) 4955.
[60] S. Bhattacharya, R.K. Mukherjee, B.K. Chaudhuri, H.D. Yang, Appl. Phys. Lett. 82 (2003) 4101.
[61] A.G. Mostafa, E.K. Abdel-Khalek, W.M. Daoush, S.F. Moustfa, J. Magn. Magn. Mater. 320 (2008) 3356.
[62] A. Banerjee, S. Pal, and B. K. Chaudhuri, J. Chem. Phys. 115, 1550 (2001).

[63] D.K. Paul, S.S. Mitra, Phys. Rev. Lett. 31 (1973) 1000.

[64] P.S. Prabhu, U.V. Varadaraju, Phys. Rev. B 53 (1996) 1146.

[65] N. F. Mott, ‘Metal-insulator transitions’ (Taylor & Francis, London, 1974).

Table 1: Correlation coefficient (R^2) in the ferromagnetic region for x = 0, based on equations (1) through (3).

Equation	(1)	(2)	(3)
(R^2)	0.64473	0.56413	0.99997

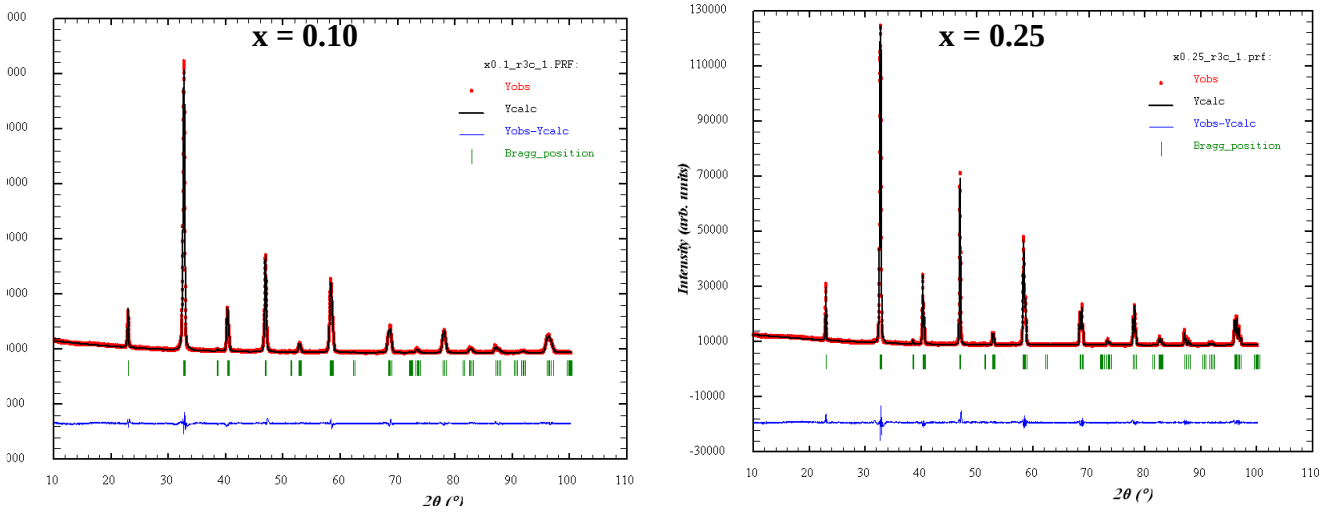

Figure 1: Observed (open symbols) and calculated (solid lines) X-ray diffraction patterns for $La_{0.6}Sr_{0.4}Mn_{1-2x}Cr_xFe_xO_3$ (x = 0.10 and 0.25).

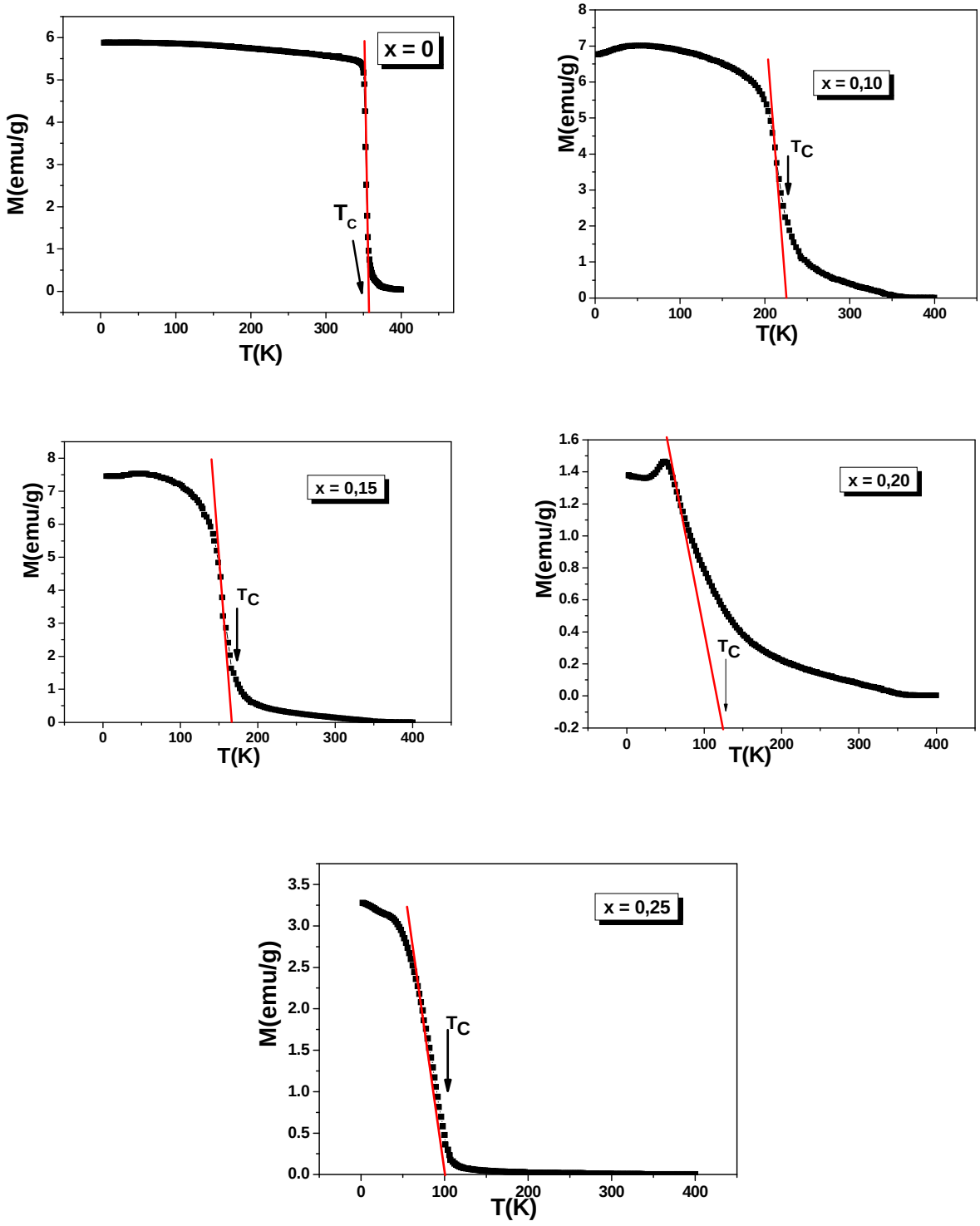

Figure 2: Temperature dependence of magnetization of $La_{0.6}Sr_{0.4}Mn_{1-2x}Fe_xCr_xO_3$ (x = 0, 0.10, 0.15, 0.20 and 0.25) with an applied field of 0.01 T.

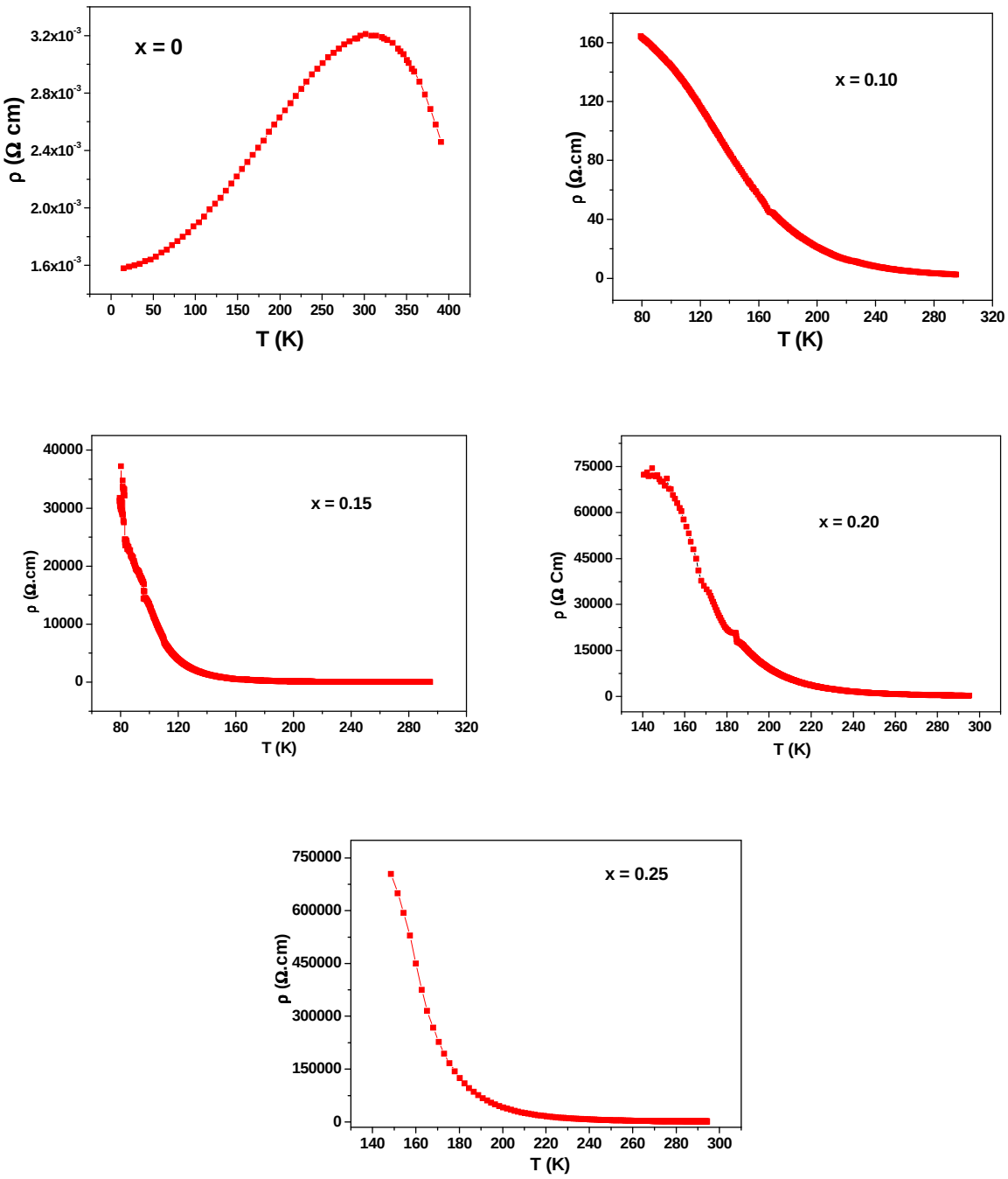

Figure 3: Temperature dependence of resistivity under zero applied field for $La_{0.6}Sr_{0.4}Mn_{1-2x}Cr_xFe_xMnO_3$ samples with x = 0.10, 0.15, 0.20 and 0.25.

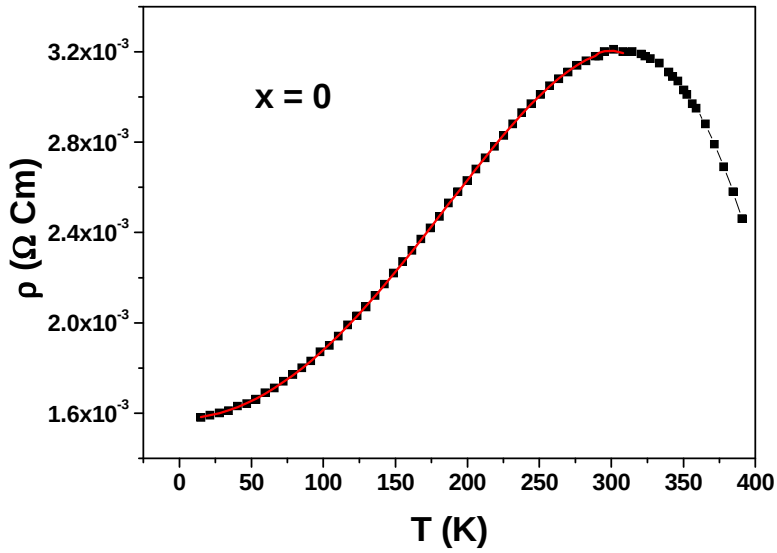

Figure 4: Fitting curve for x = 0, based on metallic behavior Eq.(3): $\rho = \rho_0 + \rho_2 T^2 + \rho_{4.5} T^{4.5}$

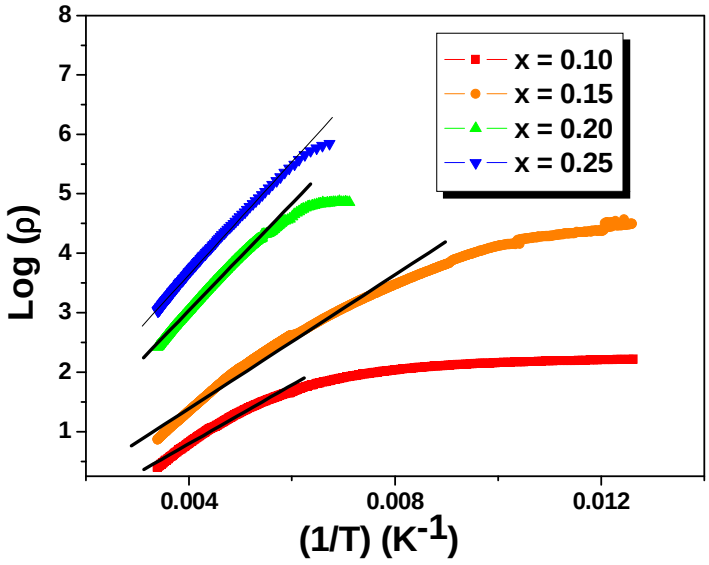

Figure 5: Plots of Log (ρ) versus (1/T) for $La_{0.6}Sr_{0.4}Mn_{1-2x}Fe_xCr_xO_3$ samples (x = 0.10, 0.15, 0.20 and 0.25). The straight lines indicate the best fit to the thermal activation (TA) model.

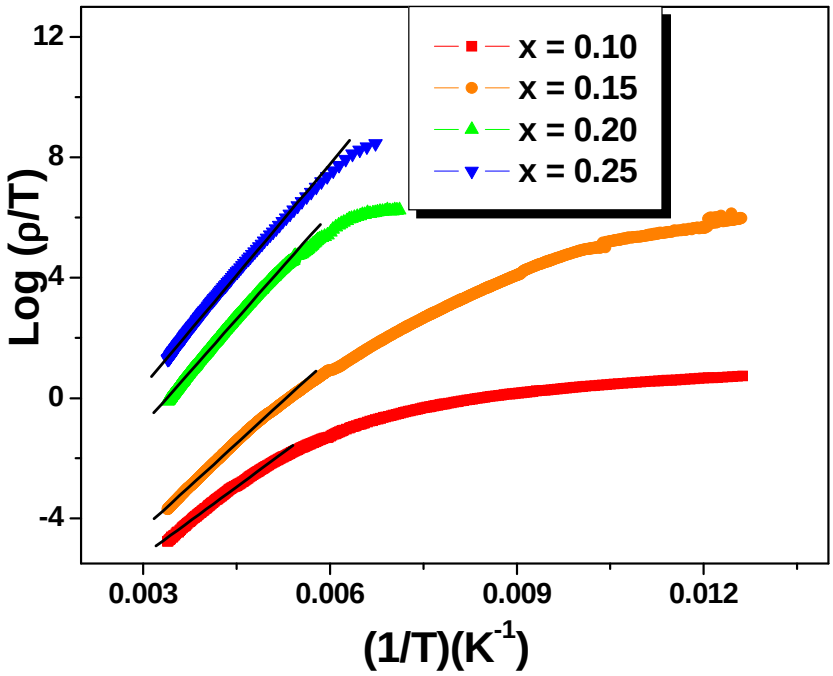

Figure 6: Plots of Log (ρ/T) versus ($1/T$) for $La_{0.6}Sr_{0.4}Mn_{1-2x}Fe_xCr_xO_3$ samples (x = 0.10, 0.15, 0.20 and 0.25). The straight lines represent the best fit to the adiabatic nearest-neighbor hopping of small polaron model (ANHSP).

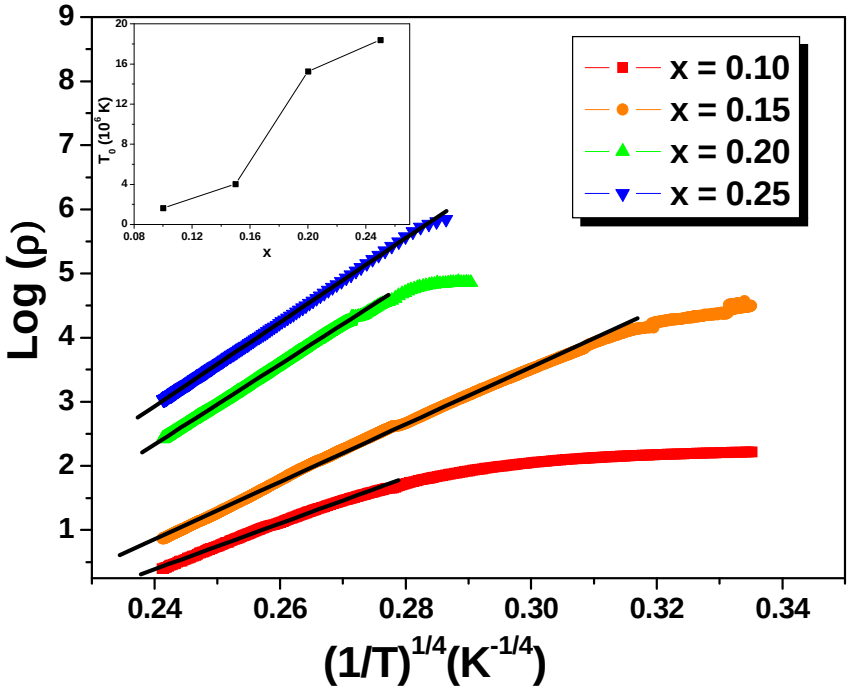

Figure 7: Plots of Log (ρ) versus $(1/T)^{1/4}$ for $La_{0.6}Sr_{0.4}Mn_{1-2x}Fe_xCr_xO_3$ samples (x = 0.10, 0.15, 0.20 and 0.25). The straight lines represent the best fit to the Mott variable range hopping (VRH) model. The inset shows the T_0 as a function of concentration x.

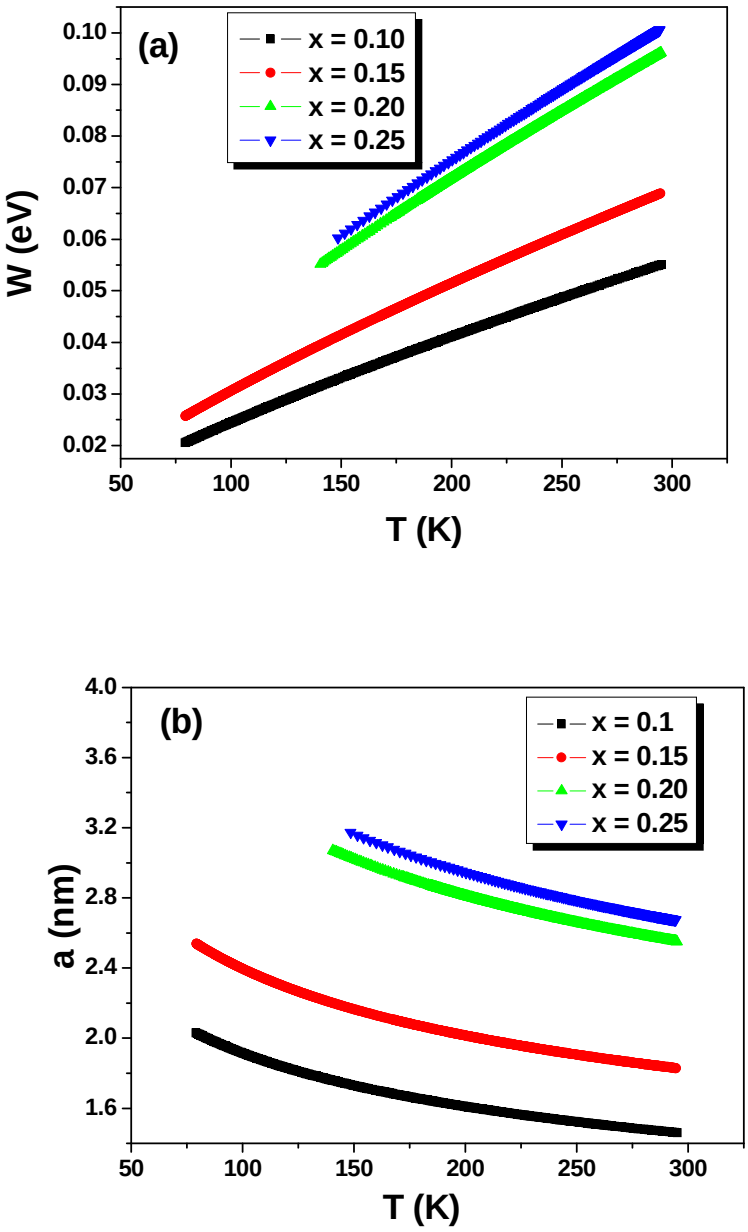

Figure 8: (a) Hopping energy W; (b) hopping distance (*a*) as a function of temperature for $La_{0.7-x}Y_xBa_{0.3}Mn_{1-x}Fe_xO_3$ samples (x = 0.10, 0.15, 0.20 and 0.25).